RSC Advances

PAPER

View Article Online
View Journal | View Issue

Cite this: *RSC Adv.*, 2018, **8**, 12900

Homogeneity and tolerance to heat of monolayer MoS_2 on SiO_2 and h-BN†

Ho-Jong Kim,[ad] Daehee Kim,[a] Suyong Jung,[a] Myung-Ho Bae,[a] Sam Nyung Yi,[b] Kenji Watanabe,[c] Takashi Taniguchi,[c] Soo Kyung Chang[d] and Dong Han Ha*[a]

Received 2nd March 2018
Accepted 26th March 2018

DOI: 10.1039/c8ra01849a

rsc.li/rsc-advances

We investigated the homogeneity and tolerance to heat of monolayer MoS_2 using photoluminescence (PL) spectroscopy. For MoS_2 on SiO_2, the PL spectra of the basal plane differ from those of the edge, but MoS_2 on hexagonal boron nitride (h-BN) was electron-depleted with a homogeneous PL spectra over the entire area. Annealing at 450 °C rendered MoS_2 on SiO_2 homogeneously electron-depleted over the entire area by creating numerous defects; moreover, annealing at 550 °C and subsequent laser irradiation on the MoS_2 monolayer caused a loss of its inherent crystal structure. On the other hand, monolayer MoS_2 on h-BN was preserved up to 550 °C with its PL spectra not much changed compared with MoS_2 on SiO_2. We performed an experiment to qualitatively compare the binding energies between various layers, and discuss the tolerance of monolayer MoS_2 to heat on the basis of interlayer/interfacial binding energy.

Introduction

Transition metal dichalcogenides (TMDCs), such as molybdenum disulfide (MoS_2), molybdenum diselenide ($MoSe_2$), tungsten disulfide (WS_2), and tungsten diselenide (WSe_2), are two-dimensional (2D) semiconducting materials with strong photoluminescence (PL) emission in the visible or near-infrared spectral regions, which makes them attractive in the development of electronic and optoelectronic devices.[1–3] TMDC monolayers exfoliated on various substrates are doped with electrons, or holes, induced by the charged impurities trapped at the TMDC-substrate interfaces. As the electrons/holes are depleted, PL emissions from TMDC monolayers are greatly enhanced in intensity and shift toward higher energies by the transformation of trions (charged excitons) into excitons.[1,4–6] Thus, PL emission has been used to analyze the local charge density, defects, and strain on TMDC monolayers in combination with the results of Raman spectroscopy.[7–13]

Properties of 2D materials depend on the number of layers, defects, substrate, and so on. Monolayer MoS_2 is a direct bandgap semiconductor with strong PL emission at 1.8–1.9 eV, while bulk MoS_2 has an indirect bandgap at an energy approximately 0.6 eV lower than the monolayer.[14,15] Photoluminescence maps of monolayer MoS_2 on SiO_2 have shown that the PL peak energy of the edges might differ from that of the crystalline basal plane (interior),[16] and moreover, thermal annealing at 450 °C or higher creates defects on its basal plane with a large enhancement of PL emission.[1,7] It has been reported that the PL/Raman properties as well as carrier mobility of MoS_2 are affected by the substrate because of the changes in the doping level, extrinsic charge trap density, and optical interference within the substrate.[17–20] In the present work, we went further to investigate the homogeneity of doping and tolerance to heat of monolayer MoS_2 on substrates SiO_2 and hexagonal boron nitride (h-BN) using PL spectroscopy. We found that monolayer MoS_2 on SiO_2 decomposed and lost its inherent crystal structure during thermal annealing up to 550 °C and subsequent optical mapping processes, while monolayer MoS_2 on h-BN, having a homogenous PL spectra over the entire area including both basal plane and edge, was well preserved. Our results are expected to be useful in the development of nano-devices that require homogeneous 2D materials and reliable functionality under harsh environmental conditions, such as high temperatures.

Experimental

MoS_2 and h-BN flakes were prepared on Si substrates capped with 300 nm-thick SiO_2 by mechanically exfoliating MoS_2 (SPI Supplies) and h-BN crystals (National Institute for Materials Science) onto the substrates. MoS_2 flakes were also prepared on SiO_2/Si substrates coated with water-soluble polystyrenesulfonic (PSS) and poly(methyl methacrylate) (PMMA). MoS_2 monolayers were identified by optical microscopy and confirmed by Raman spectroscopy. For the fabrication of MoS_2 and h-BN vertical heterostructures, MoS_2 monolayers on the

[a]*Quantum Technology Institute, Korea Research Institute of Standards and Science, Daejeon 34113, Republic of Korea. E-mail: dhha@kriss.re.kr*

[b]*Department of Electronic Material Engineering, Korea Maritime and Ocean University, Busan 49112, Republic of Korea*

[c]*National Institute for Materials Science, 1-1 Namiki, Tsukuba 305-0044, Japan*

[d]*Department of Physics, Yonsei University, Seoul 03722, Republic of Korea*

† Electronic supplementary information (ESI) available. See DOI: 10.1039/c8ra01849a

PMMA layer, obtained by removing the PSS layer, were brought into contact with thick h-BN flakes previously prepared on SiO_2 using a micro-manipulator, followed by removal of the PMMA layer with acetone.[21] The detailed fabrication process of the heterostructures is described in the ESI.† Samples were heat treated in a quartz tube (diameter = 90 mm) in a mixed atmosphere of Ar (1000 sccm) and H_2 (100 sccm). Annealing was staged and accumulated: 1 hour at 250 °C, followed by 1 hour at 450 °C, and finally 1 hour at 550 °C. After each stage, the furnace was cooled down to room temperature.

Raman and PL spectra were obtained under ambient conditions in backscattering geometry using a laser line of 532 nm as exciting light. Scattered light was analysed using a Horiba Jobin Yvon LabRAM HR spectrometer equipped with a cooled charge-coupled device. A grating of 600 grooves per mm was used for the PL experiment, while a grating of 1800 grooves per mm was used for the Raman experiment. The exciting light was focused on the samples with a diameter (full width at half maximum: FWHM) of approximately 0.65 μm using a 100× objective lens, and the total laser power on the samples was fixed below 300 μW to prevent local heating or the deterioration of sample MoS_2 by laser illumination.[9,22,23] The Si Raman peak at 520.7 cm^{-1} was used as an internal reference to calibrate the Raman peaks of MoS_2. In preliminary experiments, we monitored the PL and Raman spectra from an arbitrary point on monolayer MoS_2 for 2 hours under our experimental conditions, with no meaningful changes observed. That is, the intensities and positions of the PL and Raman peaks did not change even when the laser light continuously illuminated the same point for 2 hours, thus confirming the absence of laser heating effects on the PL and Raman spectra. Except for the acquisition time, all other experimental parameters for the PL and Raman measurements were fixed, such as confocal hole size and neutral density filter. The thickness of the h-BN flakes was measured by tapping-mode atomic force microscopy.

Results and discussion

Fig. 1(a) and (b) are optical microscopy images of MoS_2 flakes on SiO_2 and h-BN, respectively. The lower left of the MoS_2 flake on SiO_2 is monolayer, with the rest of the flake consisting of multilayer or bulk MoS_2. The MoS_2 flake on 97 nm thick h-BN is entirely monolayer except for the bottom end indicated by the arrow, with tiny yellow flakes of MoS_2 observed along the h-BN edge. Fig. 1(c) shows typical Raman spectra obtained from the basal plane of monolayer MoS_2, where two Raman peaks were observed: an $E_{2g}{}^1$ peak (in-plane vibration) and an A_{1g} peak (out-of-plane vibration).[24–26] Compared with the MoS_2 on SiO_2, we notice that both Raman peaks are shifted for MoS_2 on h-BN. It has been reported that the $E_{2g}{}^1$ peak redshifts with increasing strain[25] and likewise, an increase of the interlayer van der Waals force also redshifts the $E_{2g}{}^1$ peak due to stacking-induced structural changes or long-range coulombic interlayer interactions.[24,25,27] On the other hand, the position and FWHM of the A_{1g} peak were affected predominantly by local electron density: the peak blueshifted and sharpened with electron depletion due to reduced electron–phonon interactions,[28] although increased

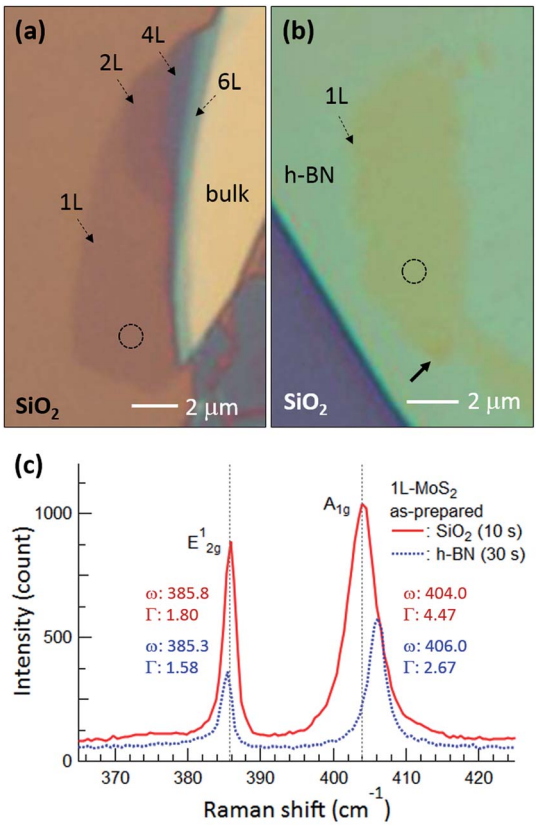

Fig. 1 Optical microscopy images of MoS_2 flakes on (a) SiO_2 and (b) h-BN, where 1L, 2L, 4L, and 6L indicate monolayer, bilayer, quadlayer, and hexalayer, respectively, estimated using the position difference between Raman $E_{2g}{}^1$ and A_{1g} peaks.[24] (c) Raman spectra of monolayer MoS_2 obtained from the dotted circles in (a) and (b). Red and blue curves and numbers represent MoS_2 on SiO_2 and h-BN, respectively, and the times in parentheses indicate the acquisition time. ω and Γ are position and FWHM of the Raman peaks. Gray dotted lines in (c) denote the positions of the $E_{2g}{}^1$ and A_{1g} peaks of monolayer MoS_2 on SiO_2.

interlayer interactions could also lead to a blueshift of the A_{1g} peak by increasing the restoring force.[26] The FWHM of the A_{1g} peak was 4.47 cm^{-1} on SiO_2 but decreased to 2.67 cm^{-1} on h-BN. The Raman spectra indicate that monolayer MoS_2 on h-BN was electron depleted compared with that on SiO_2 and/or that the monolayer MoS_2 attached more strongly to the h-BN than to the SiO_2, as discussed in detail later.

Annealing effects on the PL peak intensity (amplitude) maps of MoS_2 flakes are shown in Fig. 2. PL intensities significantly decreased with increasing thickness such that those of 6L and bulk MoS_2 appeared dark on the maps of Fig. 2(a)–(d). We noticed that the topography of the maps changed with each annealing, suggesting that the distribution of local charge density might be changed by annealing. A PL signal from MoS_2 was also observed along the edge of the thick h-BN where tiny flakes of MoS_2 were scattered.

The PL intensity of monolayer MoS_2 on SiO_2 was enhanced by approximately 20 times after annealing at 450 °C (see the scale bars next to the maps in Fig. 2). While the PL intensity of bilayer was slightly enhanced, those of multilayer and bulk were not changed on the whole, although they appear dark in

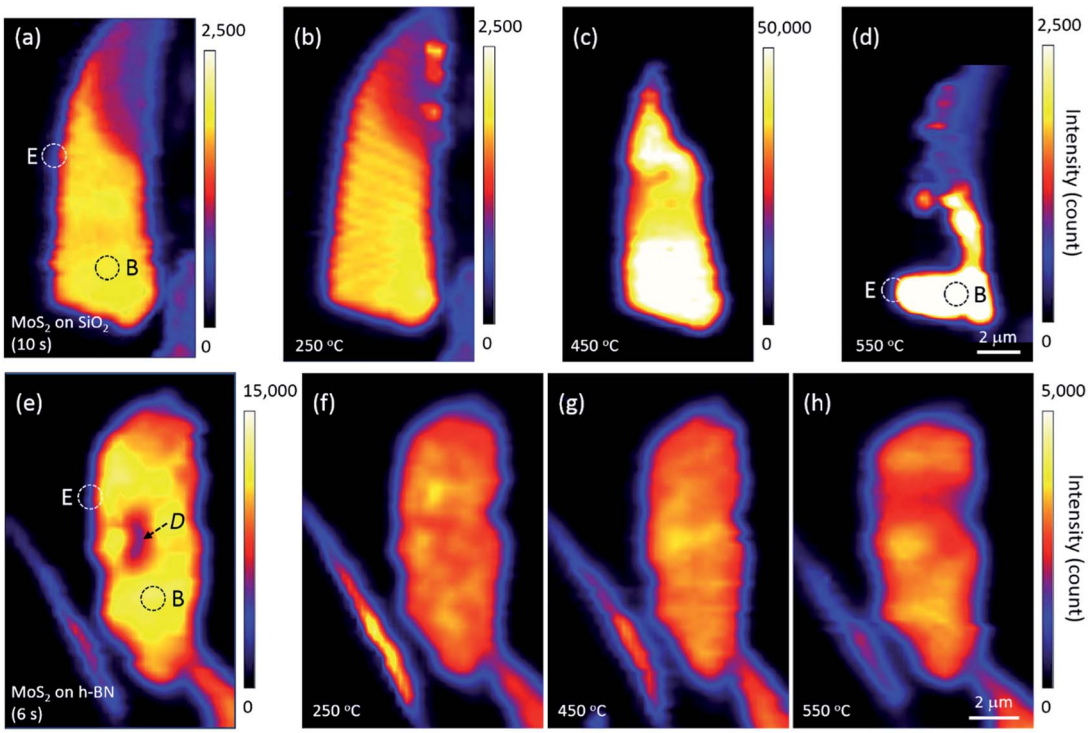

Fig. 2 Changes in the PL intensity maps of MoS_2 flakes on (a–d) SiO_2 and (e–h) h-BN upon annealing. Acquisition times for each measurement are denoted in parentheses. The mapping step was 0.25 μm, Dotted circles denote the typical edge ("E") and basal plane ("B") of monolayer MoS_2, and the dark area *D* in (e) is believed to be organic residue from the fabrication process that disappeared with annealing.

Fig. 2(c). However, the PL intensity of monolayer MoS_2 decreased significantly by annealing at 550 °C, with a large part disappearing from the PL map as shown in Fig. 2(d), indicating that monolayer MoS_2 on SiO_2 could no longer retain its intrinsic hexagonal crystal structure. Optical microscopy images showed that a part of the bilayer MoS_2 on SiO_2 was also decomposed, whereas thicker or multilayer MoS_2 was well preserved. Our results for MoS_2 on SiO_2 are consistent with the work of Liu and coworkers on oxygen etching activity with various numbers of graphene layers on SiO_2, which was discussed on the basis of substrate-induced deformations and preexisting defects;[29] they showed that oxidative etching proceeded faster in single layers than in multi-layers during annealing in an O_2/Ar gas flow, and moreover, etching did not occur on the defect-free basal plane of triple or thicker layer graphene at or below 600 °C.

Many experimental results have shown that defects can be created in monolayer MoS_2 on SiO_2 *via* thermal annealing, plasma treatment, electron/ion irradiation, or laser irradiation.[1,2,7,8,30] Moreover, high-resolution transmission electron microscopy images have verified S-vacancies—the most common type of defect—in electron-irradiated monolayer MoS_2.[31] Tongay, Nan, and their coworkers also reported that thermal annealing at 450 °C or higher creates S-vacancies by breaking the S–Mo–S bonds of MoS_2.[1,7] Annealing at 550 °C removes even more S atoms, such that monolayer MoS_2 is considered to be fragmented into nano-domains that can be easily decomposed by laser light; this is in contrast to thicker or multilayer MoS_2 in which all atoms are bonded horizontally and vertically. Here, Fig. 2 suggests that the interfacial interaction between MoS_2 and SiO_2 is weaker than the interlayer interaction between layers of MoS_2 because of impurities at the MoS_2–SiO_2 interface and SiO_2 surface roughness.[19–21] Previous results on the comparison of binding energies between the interlayer/interface support our results. The interlayer binding energy between MoS_2 layers calculated using advanced density-functional theory was 330 mJ m^{-2}, and the energy required to peel off a single layer from the surface of a multilayer structure increased with the number of layers.[32] On the other hand, the interfacial binding energy of MoS_2 on SiO_2 substrates measured by Deng and coworkers was 170 mJ m^{-2}.[33]

We argue that the tolerance of monolayer MoS_2 to heat is influenced by the interlayer/interfacial binding energy as well as the interatomic bonding forces in the layer. In fact, monolayer MoS_2 on h-BN was well preserved even after annealing at 550 °C and subsequent PL mapping. Fig. 2 strongly indicates that due to the atomically flat, impurity-free surface of newly exfoliated h-BN,[19,21] interfacial binding between MoS_2 and h-BN is stronger than that between MoS_2 and SiO_2, which is consistent with the results of the Raman experiments shown in Fig. 1(c). Our results are in good agreement with the dependence of MoS_2 interfacial binding energy on substrate roughness as measured by Deng and coworkers.[33] Strong interfacial binding is considered to enhance the tolerance of monolayer MoS_2 on h-BN to heat.

To support our argument, we performed an experiment to qualitatively compare the binding energies between the various

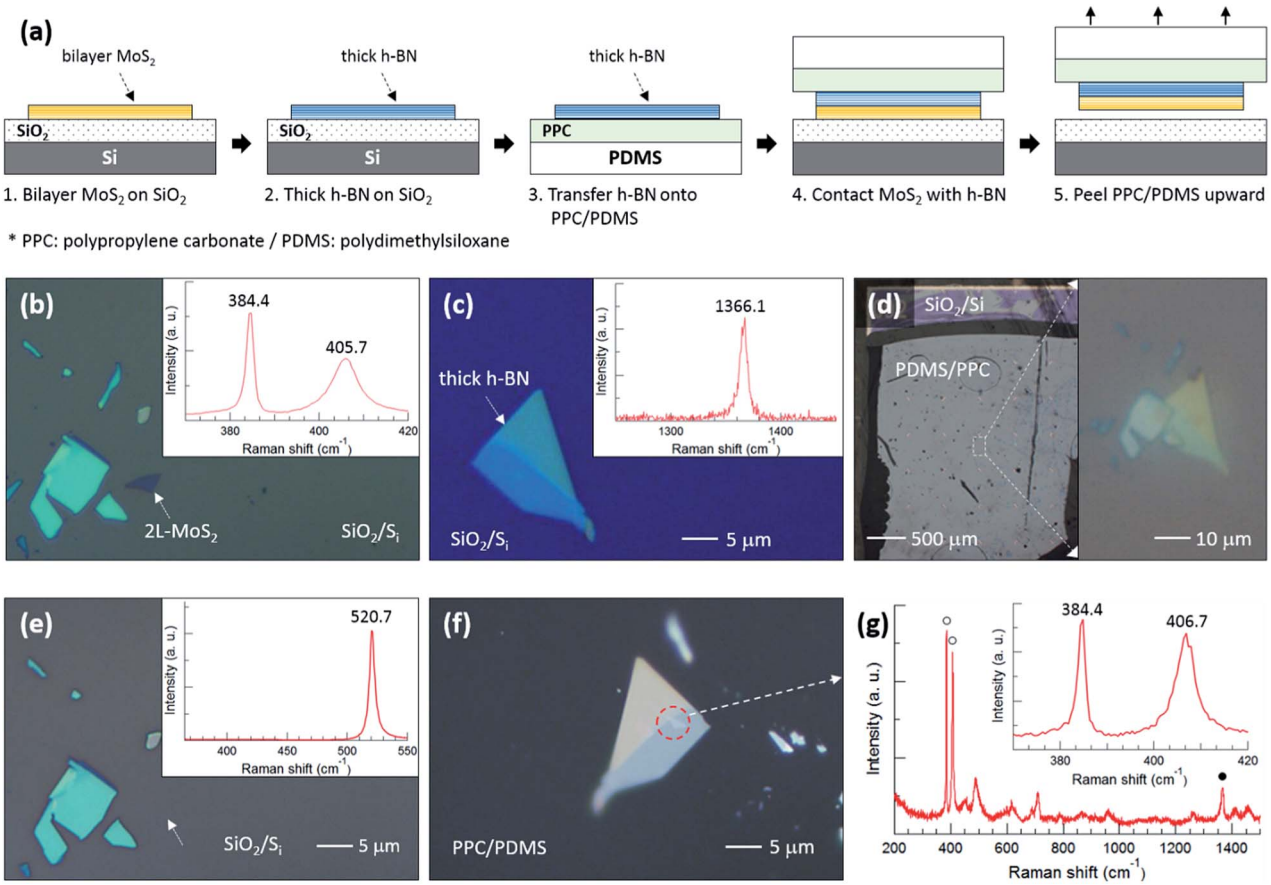

Fig. 3 (a) Schematic diagram of the experimental process to qualitatively compare the binding energies between various layers. (b and c) Optical microscopy images with corresponding Raman spectra for steps 1 and 2 in (a), respectively. (d) Optical microscopy image for steps 3 and 4 in (a). The right image is an enlargement of the white rectangular region on the left. (e and f) Optical microscopy images for the lower and upper sections of step 5 in (a), respectively, with corresponding Raman spectrum in (e). (g) Raman spectrum obtained from the red dotted circle in (f).

layers as summarized in Fig. 3. The flake designated by a white dotted arrow in Fig. 3(b) is bilayer MoS_2, the thickness of which was determined using the position difference between the $E_{2g}{}^1$ and A_{1g} peaks in the inset Raman spectrum. The h-BN flake in Fig. 3(c) was also confirmed using the Raman spectrum. Fig. 3(d) shows optical images of PDMS/PPC/h-BN placed on $MoS_2/SiO_2/Si$; the right image demonstrates that the thick h-BN is precisely positioned on the bilayer MoS_2. Fig. 3(e) shows that the bilayer MoS_2 was completely separated from SiO_2, as only a single Si Raman peak at 520.7 cm^{-1} was observed from the position where bilayer MoS_2 was located. The bilayer MoS_2 flake was then transferred onto the thick h-BN, as can be observed in the red dashed circle in Fig. 3(f), after peeling PDMS/PPC upward. In the Raman spectrum of Fig. 3(g) obtained from the red dashed circle, open (closed) circles denote Raman peaks of bilayer MoS_2 (h-BN), while other peaks are from the PDMS/PPC. The inset in Fig. 3(g) shows the Raman spectrum of the MoS_2 flake in detail. The A_{1g} peak at higher frequency was blueshifted but the position of the $E_{2g}{}^1$ peak at lower frequency was unchanged compared with those of the MoS_2 flake on SiO_2, indicating a depletion of electrons from MoS_2 on h-BN compared with that on SiO_2. The position difference between the $E_{2g}{}^1$ and A_{1g} peaks verifies that it is bilayer—not monolayer—MoS_2. That is, bilayer MoS_2 was not separated between the layers of MoS_2 nor at the interface between MoS_2 and h-BN, but rather was separated at the interface between MoS_2 and SiO_2. Our results demonstrate that the MoS_2–SiO_2 interfacial binding energy is weaker than the MoS_2–MoS_2 interlayer binding energy as well as the MoS_2–h-BN interfacial binding energy.

Fig. 4 displays PL spectra obtained from the typical edge and basal plane of monolayer MoS_2 on SiO_2 and h-BN. Compared with the PL spectrum of the as-prepared MoS_2 on SiO_2, that of MoS_2 on h-BN greatly increased in intensity even though the acquisition time was reduced from 10 to 6 s; further, the PL peak due to valence band splitting disappeared.[6,14] Moreover, the peak position shifted from 1.83 to 1.89 eV and the FWHM decreased from 0.11 to 0.04 eV on h-BN, verifying that MoS_2 on h-BN was electron depleted compared with that on SiO_2 due to the impurity-free surface of h-BN.[1,4,19]

The basal plane of the as-prepared monolayer MoS_2 on SiO_2 had a PL maximum of negatively charged trions at approximately 1.83 eV, whereas the edge had a single PL peak of excitons at approximately 1.87 eV. This can be ascribed to local electron depletion by foreign molecules adsorbed on the dangling bonds along the edge. The edge was defined as the

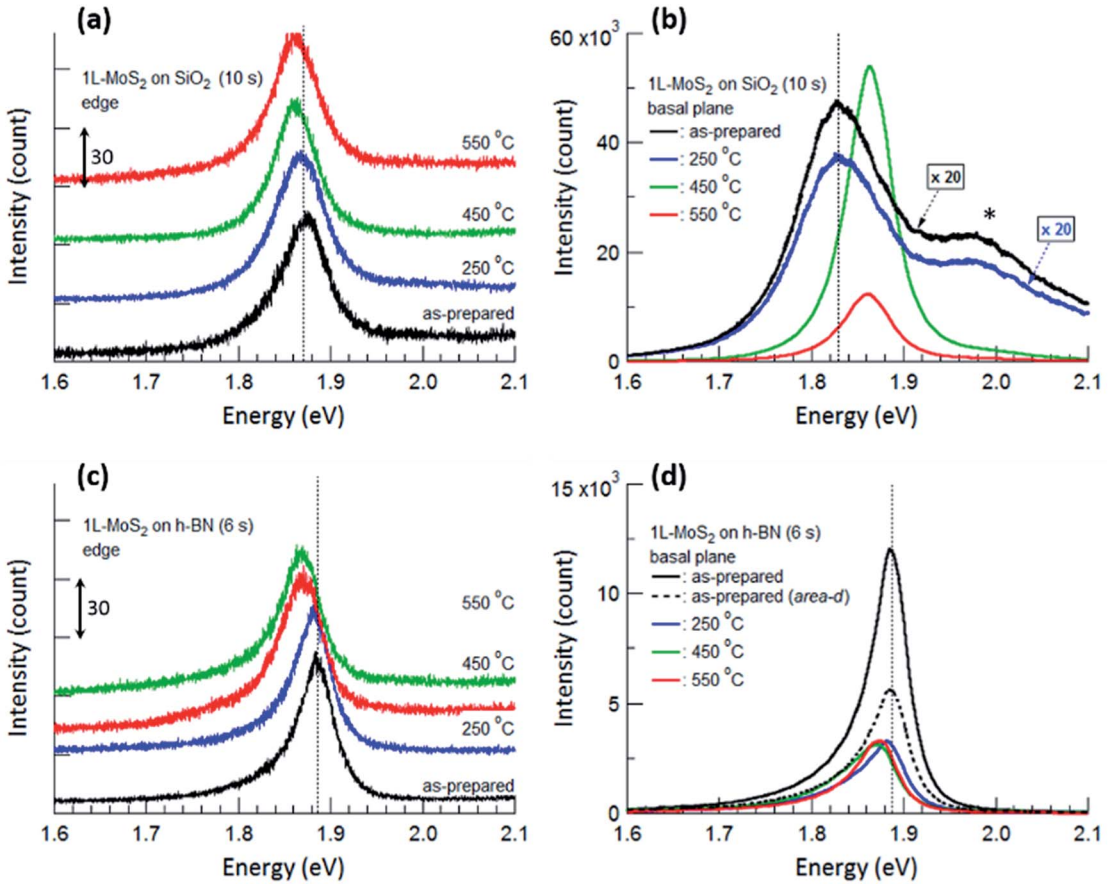

Fig. 4 PL spectra obtained from the edge (a and c) and basal plane (b and d) of monolayer MoS_2 shown in Fig. 2. The PL spectra of as-prepared MoS_2 and MoS_2 annealed at 250 °C are multiplied by 20 in (b). The shoulder peak at 1.98 eV marked by an asterisk in (b) is due to the splitting of the monolayer MoS_2 valence band. PL spectra obtained from the edges are shifted vertically for ease of viewing, and the unit value of the *Y*-axis in (a) and (c) is 30 count. The times in parentheses denote the acquisition time for each measurement. Vertical dotted lines denote the PL peak positions of the as-prepared MoS_2 monolayers.

points corresponding to the initial upturns of the PL intensity profiles across the edge of MoS_2 (to be precise, the PL signal of the edge is the sum of the signals from the true edge and the basal plane near the edge since the laser light has a finite size). The difference in PL spectra between the basal plane and the edge of MoS_2 on SiO_2 was evident even after annealing at 250 °C. However, annealing at 450 °C resulted in remarkable changes in the PL spectrum of the basal plane *via* the chemisorption of foreign molecules, such as O_2 and H_2, at newly created defects; such changes include a shift of the peak position to approximately 1.86 eV, an increase in the peak intensity by more than 20 times, and the disappearance of the shoulder peak at 1.98 eV. On the other hand, the PL peak of the edge only slightly shifted toward a lower energy, such that both PL spectra of the basal plane and edge of MoS_2 on SiO_2 had a single peak at the same position of approximately 1.86 eV.

For monolayer MoS_2 on h-BN, both PL peaks of the basal plane and edge of MoS_2 unexpectedly had maxima at the same energy, as shown in Fig. 4(c) and (d), even though foreign molecules were considered to be chemisorbed on the edge. This tendency was not changed by thermal annealing up to 550 °C. Fig. 4 indicates that the PL properties and doping of electron-depleted MoS_2 on h-BN is insensitive to the adsorption of electron-accepting molecules, which is contrary to the case of monolayer MoS_2 on SiO_2. In other words, electron transfer from the electron-depleted MoS_2 to the adsorbed molecules is considered to be insignificant compared with that from MoS_2 on SiO_2, on which the electron transfer from an S-vacancy of MoS_2 to a chemisorbed O_2 molecule reaches 0.997 *e*.[7] Our results show that with or without annealing, local electron density was nearly homogeneous over the entire monolayer MoS_2 on h-BN, including both basal plane and edge.

Thermal annealing decreased the PL intensity of monolayer MoS_2 on h-BN; in addition, the PL peaks of both the basal plane and edge of MoS_2 shifted toward a lower energy. First-principle calculations showed that both O_2 and H_2 molecules physisorbed on monolayer MoS_2 act as electron acceptors with charge transfer values of 0.04 *e* and 0.004 *e* for O_2 and H_2, respectively. In addition, the adsorption energies for O_2 and H_2 on ideal MoS_2 were calculated to be −116 and −82 meV.[34] Replacing some O_2 molecules physisorbed on the basal plane of MoS_2 with H_2 molecules during annealing in a H_2/Ar gas flow could increase the local electron density on the basal plane, resulting in the changes in the intensity and position of PL

spectrum. Our results show that the electron-depleted MoS_2 on h-BN responds to the substitution of O_2 with H_2 which results in the electron-doping, although it was insensitive to the adsorption of electron-accepting molecules. Nevertheless, we consider that few of the O_2 molecules chemisorbed on the edge or other defects could be removed during thermal annealing since the binding energy of an O_2 molecule on an S-vacancy of MoS_2 calculated by first-principle method is −2.395 eV.[7]

Conclusions

The PL spectra of the edge for the as-prepared MoS_2 on SiO_2 differed in peak position and shape from those of the basal plane, but annealing at 450 °C rendered the PL spectra homogeneous by creating many defects on the basal plane. On the other hand, MoS_2 on h-BN demonstrated a homogenous PL spectra over the entire area regardless of annealing, although foreign molecules were expected to chemisorb to the dangling bonds along the edge. Electron-depleted MoS_2 on h-BN responded to the adsorption of foreign molecules which results in the electron-doping, while it was insensitive to the adsorption of electron-accepting molecules. Monolayer MoS_2 on SiO_2 was further decomposed and almost lost its inherent crystal structure during thermal annealing at 550 °C and subsequent optical mapping process, while monolayer MoS_2 was well preserved on h-BN. We contend that the tolerance of monolayer MoS_2 to heat is influenced by interlayer/interfacial binding energy as well as the interatomic bonding forces in the layer, strongly supported by experimental results on the comparison of binding energies between various layers.

Conflicts of interest

There are no conflicts to declare.

Acknowledgements

This research was supported by the National Research Foundation of Korea (NRF) (Grant No. 2015R1A2A1A10056103) funded by the Ministry of Education, and also supported by the Korea-Hungary joint laboratory program for Nanosciences through the National Research Council of Science and Technology.

References

1 S. Tongay, J. Zhou, C. Ataca, J. Liu, J. S. Kang, T. S. Matthews, L. You, J. Li, J. C. Grossman and J. Wu, *Nano Lett.*, 2013, **13**, 2831–2836.
2 S. Tongay, J. Suh, C. Ataca, W. Fan, A. Luce, J. S. Kang, J. Liu, C. Ko, R. Raghunathanan, J. Zhou, F. Ogletree, J. Li, J. C. Grossman and J. Wu, *Sci. Rep.*, 2013, **3**, 2657.
3 F. Xia, H. Wang, D. Xiao, M. Dubey and A. Ramasubramaniam, *Nat. Photonics*, 2014, **8**, 899–907.
4 S. Mouri, Y. Miyauchi and K. Matsuda, *Nano Lett.*, 2013, **13**, 5944–5948.
5 N. Scheuschner, O. Ochedowski, A.-M. Kaulitz, R. Gillen, M. Schleberger and J. Maultzsch, *Phys. Rev. B*, 2014, **89**, 125406.
6 J. S. Ross, S. Wu, H. Yu, N. J. Ghimire, A. M. Jones, G. Aivazian, J. Yan, D. G. Mandrus, D. Xiao, W. Yao and X. Xu, *Nat. Commun.*, 2013, **4**, 1474.
7 H. Nan, Z. Wang, W. Wang, Z. Liang, Y. Lu, Q. Chen, D. He, P. Tan, F. Miao, X. Wang, J. Wang and Z. Ni, *ACS Nano*, 2014, **8**, 5738–5745.
8 H. M. Oh, G. H. Han, H. Kim, J. J. Bae, M. S. Jeong and Y. H. Lee, *ACS Nano*, 2016, **10**, 5230–5236.
9 E. Kim, C. Ko, K. Kim, Y. Chen, J. Suh, S.-G. Ryu, K. Wu, X. Meng, A. Suslu, S. Tangay, J. Wu and C. P. Grigoropoulos, *Adv. Mater.*, 2016, **28**, 341–346.
10 H. R. Gutiérrez, N. Perea-López, A. L. Elías, A. Berkdemir, B. Wang, R. Lv, F. López-Urías, V. H. Crespi, H. Terrones and M. Terrones, *Nano Lett.*, 2013, **13**, 3447–3454.
11 W. Shi, M.-L. Lin, Q.-H. Tan, X.-F. Qiao, J. Zhang and P.-H. Tan, *2D Mater.*, 2016, **3**, 025016.
12 A. Michail, N. Delikoukos, J. Parthenios, C. Galiotis and K. Papagelis, *Appl. Phys. Lett.*, 2016, **108**, 173102.
13 W. Su, H. Dou, J. Li, D. Huo, N. Dai and L. Yang, *RSC Adv.*, 2015, **5**, 82924–82929.
14 A. Splendiani, L. Sun, Y. Zhang, T. Li, J. Kim, C.-Y. Chim, G. Galli and F. Wang, *Nano Lett.*, 2010, **10**, 1271–1275.
15 K. F. Mak, C. Lee, J. Hone, J. Shan and T. F. Heinz, *Phys. Rev. Lett.*, 2010, **105**, 136805.
16 A. M. van der Zande, P. Y. Huang, D. A. Chenet, T. C. Berkelbach, Y. You, G.-H. Lee, T. F. Heinz, D. R. Reichman, D. A. Muller and J. C. Hone, *Nat. Mater.*, 2013, **12**, 554–561.
17 Y. Li, Z. Qi, M. Liu, Y. Wang, X. Cheng, G. Zhang and L. Sheng, *Nanoscale*, 2014, **6**, 15248–15254.
18 M. Buscema, G. A. Steele, H. S. J. van der Zant and A. Castellanos-Gomez, *Nano Res.*, 2014, **7**, 561–571.
19 M. Y. Chan, K. Komatsu, S.-L. Li, Y. Xu, P. Darmawan, H. Kuramochi, S. Nakaharai, A. Aparecido-Ferreira, K. Watanabe, T. Taniguchi and K. Tsukagoshi, *Nanoscale*, 2013, **5**, 9572–9576.
20 Y. Guo, X. Wei, J. Shu, B. Liu, J. Yin, C. Guan, Y. Han, S. Gao and Q. Chen, *Appl. Phys. Lett.*, 2015, **106**, 103109.
21 C. R. Dean, A. F. Young, I. Meric, C. Lee, L. Wang, S. Sorgenfrei, K. Watanabe, T. Taniguchi, P. Kim, K. L. Shepard and J. Hone, *Nat. Nanotechnol.*, 2010, **5**, 722–726.
22 S. Sahoo, A. P. S. Gaur, M. Ahmadi, M. J.-F. Guinel and R. S. Katiyar, *J. Phys. Chem. C*, 2013, **117**, 9042–9047.
23 N. Lundt, E. Cherotchenko, O. Iff, X. Fan, Y. Shen, P. Bigenwald, A. V. Kavokin, S. Höfling and C. Schneider, *Appl. Phys. Lett.*, 2018, **112**, 031107.
24 C. Lee, H. Yan, L. E. Brus, T. F. Heinz, J. Hone and S. Ryu, *ACS Nano*, 2010, **4**, 2695–2700.
25 C. Rice, R. J. Young, R. Zan, U. Bangert, D. Wolverson, T. Georgiou, R. Jalil and K. S. Novoselov, *Phys. Rev. B*, 2013, **87**, 081307(R).
26 A. G. Bagnall, W. Y. Liang, E. A. Marseglia and B. Welber, *Physica B+C*, 1980, **99**, 343–346.

27 B. Chakraborty, H. S. S. Ramakrishna Matte, A. K. Sood and C. N. R. Rao, *J. Raman Spectrosc.*, 2013, **44**, 92–96.
28 B. Chakraborty, A. Bera, D. V. S. Muthu, S. Bhowmick, U. V. Waghmare and A. K. Sood, *Phys. Rev. B*, 2012, **85**, 161403(R).
29 L. Liu, S. Ryu, M. R. Tomasik, E. Stolyarova, N. Jung, M. S. Hybertsen, M. L. Steigerwald, L. E. Brus and G. W. Flynn, *Nano Lett.*, 2008, **8**, 1965–1970.
30 S. Mignuzzi, A. J. Pollard, N. Bonini, B. Brennan, I. S. Gilmore, M. A. Pimenta, D. Richards and D. Roy, *Phys. Rev. B*, 2015, **91**, 195411.
31 H.-P. Komsa, J. Kotakoski, S. Kurasch, O. Lehtinen, U. Kaiser and A. V. Krasheninnikov, *Phys. Rev. Lett.*, 2012, **109**, 035503.
32 T. Björkman, A. Gulans, A. V. Krasheninnikov and R. M. Nieminen, *Phys. Rev. Lett.*, 2012, **108**, 235502.
33 S. Deng, E. Gao, Z. Xu and V. Berry, *ACS Appl. Mater. Inter.*, 2017, **9**, 7812–7818.
34 Q. Yue, Z. Shao, S. Chang and J. Li, *Nanoscale Res. Lett.*, 2013, **8**, 425.